Progress In Electromagnetics Research, Vol. 106, 279–293, 2010

IMPROVED CURRENT DECOMPOSITION IN HELICAL ANTENNAS USING THE ESPRIT ALGORITHM

Y. Li and H. Ling

Department of Electrical and Computer Engineering
The University of Texas at Austin
Austin, TX 78712-1084, USA

Abstract—We apply the ESPRIT algorithm to decompose the currents on a helical antenna into different traveling wave modes. The strengths, phase velocities and decay constants of the various modes are extracted across frequencies. Their contributions to the antenna performance including gain, polarization and time-domain radiated pulse shape are investigated. Our results show that the T_0^+ mode is a dominant contributor to the helix gain at the low end of the frequency band while the T_1^+ mode contributes significantly to the gain at higher frequencies. It is also found that the reflected current modes from the open end reduce the circular polarization purity of the helix. Lastly, it is observed that the T_1^+ and T_0^+ modes contribute constructively to a low-dispersion pulse from the antenna.

1. INTRODUCTION

The endfire mode (or axial mode) helical antenna is widely used for its high gain, good circular polarization and wide bandwidth. The operating principles of the endfire-mode helix have been extensively investigated and are considered well-understood. In this mode of operation, the dominant traveling wave mode is T_1^+, which satisfies the Hansen-Woodyard condition in the end-fire direction [1–3]. More recently, the helical antenna has been considered in the high power microwave community as a potential candidate for pulse power radiation [4, 5]. This application utilizes the advantages of the helix such as high power handling capability, compact size, and orientation independence for penetrating gaps. Motivated by this application, we set out to re-examine the helix structure, in particular the time domain radiated pulse from this well-known antenna.

Received 28 May 2010, Accepted 19 July 2010, Scheduled 25 July 2010
Corresponding author: Y. Li (yangl@mail.utexas.edu).

One effective approach to understand the operating principle of the helix is to identify various traveling wave modes excited on the helix. In addition to the dominant T_1^+ mode, there are also other modes including T_0^+, T_2^+ as well as the corresponding reflected components T_1^-, T_0^- and T_2^- from the open end of the helix. These modes can be studied rigorously by considering the helix as an infinite periodic structure [6, 7]. However, the excitation strength of these modes cannot be obtained in this manner. Using a phase slope fitting approach, Marsh [8] decomposed the measured current on a helical antenna into different modes and explained the antenna performance using the dominant current component. However, the resulting current decomposition was only qualitative. To better understand the effect of the other current modes on the performance of the helical antenna, an improved current decomposition is desirable.

In this paper, we present an improved mode decomposition of the helix current by applying the Estimation of Signal Parameters via Rotational Invariance Technique (ESPRIT) [9, 10]. ESPRIT is a super-resolution spectral estimation algorithm which has been applied previously to wave propagation problem with good success [11, 12]. It offers better robustness to noise than Prony's method [13]. It has the same super resolution properties as MUSIC [14] but is more computationally efficient. By using ESPRIT, an improved mode decomposition of helix current can be obtained and each current mode's magnitude, phase velocity, and decay constant can be estimated. Based on the improved current decomposition, a better understanding of the effects of different current modes on the antenna performance, in particular for wideband pulse radiation, can be achieved.

This paper is organized as follows. In Section 2, the ESPRIT algorithm is introduced and applied to decompose the helix current at various frequencies. The phase velocities of the three dominant modes are extracted across frequencies. In Section 3, the effects of each current mode on antenna performances including gain and polarization are investigated. In Section 4, the time domain radiation characteristics of the helix are studied and explained based on the contribution from each current mode's time domain radiation. Section 5 summarizes this paper. Simulated current data from the Numerical Electromagnetics Code (NEC) are used throughout the paper.

2. CURRENT DECOMPOSITION VIA ESPRIT

To illustrate the current decomposition using ESPRIT, we first simulate the current distribution along an 8-turn, right-handed helix

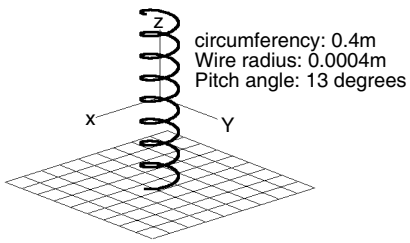

Figure 1. An 8-turn helical antenna prototype.

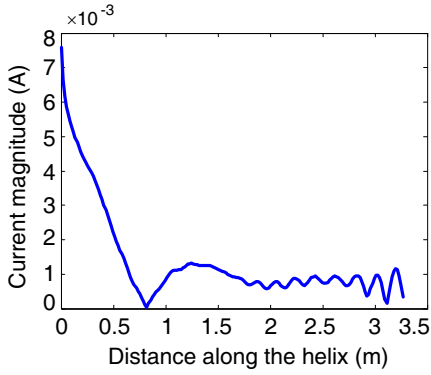

Figure 2. Current distribution at 750 MHz.

antenna using NEC. Nominal design numbers are used for the axial mode helix. Fig. 1 shows the geometry of the helix antenna. The center frequency is 750 MHz. The circumference of the helix is one wavelength and the wire radius is 0.001 wavelength, both at the center frequency. The pitch angle is 13 degrees. An infinitely PEC ground plane is assumed in the simulation. Fig. 2 plots the simulated current distribution along the helix structure at 750 MHz.

The above NEC simulated current are total current flowing along the helix structure. By decomposing the total current into various forward and backward traveling wave modes, we can better investigate each mode's contribution to the antenna performance and gain more physical insights into the antenna working principles. Therefore, next we model the current distribution on the helical antenna as a summation of N current modes, each with a distinct wave number β_n, (or the corresponding wave velocity $v_n{=}2\pi f/\beta_n$), attenuation constant α_n and a complex strength c_n:

$$J(\xi) = \sum_n c_n e^{-j\beta_n \xi - \alpha_n \xi} \tag{1}$$

where ξ is the length parameter measured along the helix winding. To determine β, α and c from the observed current, the ESPRIT algorithm is applied to the simulated current one frequency at a time. ESPRIT [9] was originally developed as a Direction-of-Arrival (DOA) estimation algorithm. It is based on the data model:

$$y(\xi_i) = \sum_{k=1}^{d} a_k e^{j\beta_k \xi_i} + n(\xi_i) \quad i = 1, 2, \ldots, N \tag{2}$$

where n is additive white noise. Given $N > 2d + 1$, ESPRIT can estimate d, a_k and β_k without error. Therefore, ESPRIT is an eigenspace parameter estimator that estimates a set of β_n, α_n in Eq. (1) based on the generalized singular value decomposition of the covariance matrix. Once they are estimated, c_n can be found by the total least-squares criterion to arrive at the best fit of the total current J. In applying ESPRIT, we use the maximum model order $N/2$ to achieve a good fit to the data, where N $(= 41)$ is the total number of data samples. Fig. 3(a) plots the extracted wave velocity of the four dominant modes. The vertical axis shows the phase velocity scale, which has been normalized to the speed of light in free space. The horizontal axis shows the distance along the helix winding (ξ). The color in the plot indicates the strength of the each current mode versus distance, $c_n e^{-\alpha_n \xi}$, displayed on a decibel scale. The change of the current mode strength along the helix winding is clearly seen. In Fig. 3(b), it is shown that the sum of the four dominant modes accurately reconstructs the original simulated current distribution. At this frequency, higher order modes are much weaker and can be neglected.

In Fig. 3(a), T_0^+ and T_1^+ are the positive traveling current modes while T_0^- and T_1^- are the corresponding reflected current modes from the open end. It is seen that the magnitude of T_1^+ is almost constant along the helix and its phase velocity is smaller than that of the free space. This is the familiar slow wave on the helix and is typically considered the dominant radiation mode in the literature [8]. We also observe that at this frequency, T_0^+ exhibits a larger phase

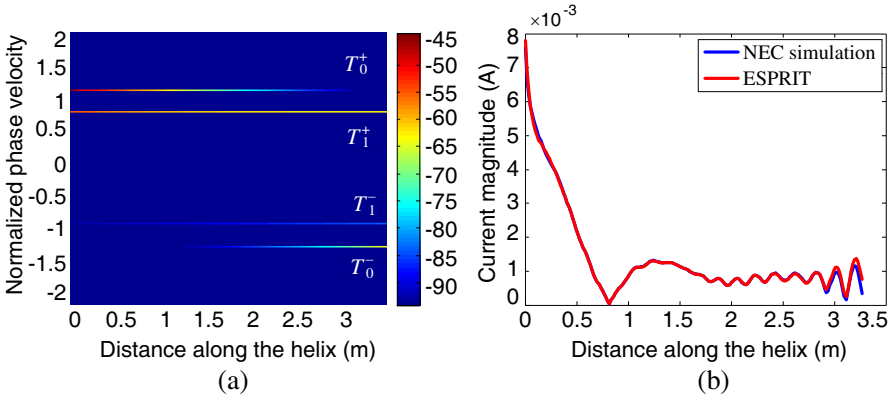

Figure 3. (a) ESPRIT decomposition at 750 MHz. (b) ESPRIT fitting at 750 MHz.

velocity but decays much faster than the T_1^+ mode. The phase velocities of the reflected waves T_0^- and T_1^- are equal and opposite of their corresponding positive traveling counterparts. However, their magnitudes are much weaker.

The helix current distributions at the low frequency end of 550 MHz and at the high frequency end of 950 MHz are similarly simulated using NEC and decomposed using ESPRIT. Figs. 4(a) and 5(a) show respectively the decomposed current modes at 550 MHz and 950 MHz. Figs. 4(b) and 5(b) show respectively the reconstruction of the currents at both frequencies. Both reconstructed currents agree well with the original simulation. At 550 MHz, the dominant

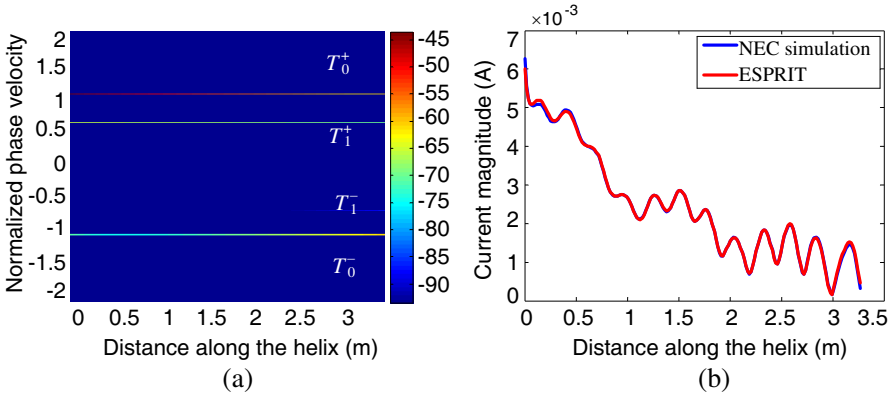

Figure 4. (a) ESPRIT decomposition at 550 MHz. (b) ESPRIT fitting at 550 MHz.

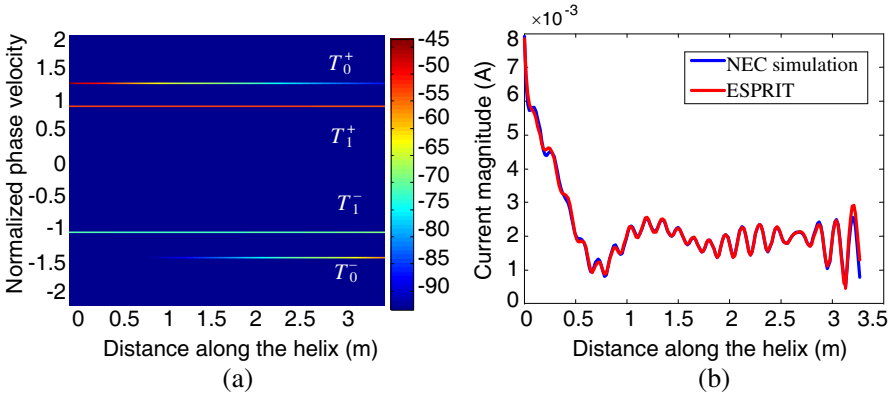

Figure 5. (a) ESPRIT decomposition at 950 MHz. (b) ESPRIT fitting at 950 MHz.

mode is the fast wave T_0^+ while the slow wave T_1^+ is only weakly excited. At 950 MHz, the strength of T_1^+ is strong and slowly decaying. Consequently, the reflected mode T_1^- persists over the entire length of the helix.

We also notice the phase velocities of the current modes change as a function of frequency. To illustrate such frequency dependence, the phase velocities of different current modes are extracted from 500 MHz to 1000 MHz and plotted in Fig. 6. It is well known that, the phase velocity of the dominant wave propagation on the helix is such that the phase delay between turns fulfils the Hansen-Woodyard (increased-directivity) condition [2]. In Fig. 6, our extracted phase velocity of T_1^+ confirms this conclusion, as it shows good agreement with the phase velocity track required by the Hansen-Woodyard condition, which is plotted as the dashed line. For the T_0^+ mode, the phase velocity increases as the frequency goes up and can be greater than the speed of light in free space. This observation is somewhat contrary to that previous reported in the literature [2, 8], in which the speed of T_0^+ is assumed to be equal to the speed of light in free space. For the T_2^+ mode, which has previously been observed in measurements only when the circumference is larger than 1.4 wavelengths [2], can be observed at 850 MHz, where the circumference is equal to 1.1 wavelengths.

3. EFFECTS OF CURRENT MODES ON GAIN AND POLARIZATION

Based on the above improved current decomposition of the helix, we next study the effects of different current modes on the gain and polarization of the helical antenna in this section.

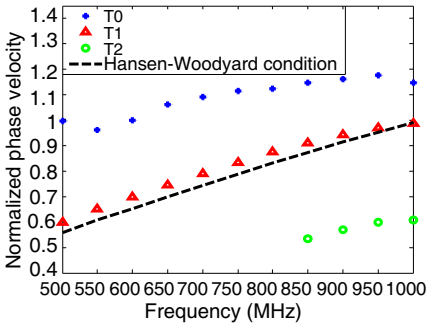

Figure 6. Phase velocities of different current modes.

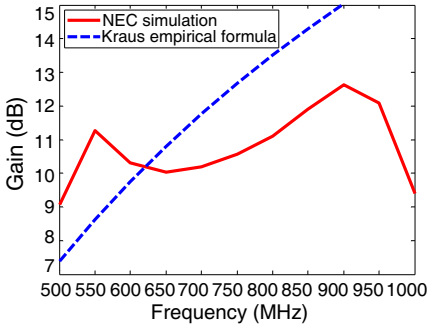

Figure 7. Gain of the 8-turn helical antenna.

3.1. Gain

An axial mode helix is known to have relatively high gain in the endfire direction across a wide bandwidth. Many simulations and measurements have been carried out to study the gain of the helical antenna. However, some results could not be explained by the T_1^+ slow wave, which was assumed to be the dominant radiation mode of the helix. As an example, it was found in [15] that the gain of a balanced helix at the center frequency is smaller than that at lower frequencies. To illustrate this, we simulate the gain of the above 8-turn helical antenna from 500 MHz to 1000 MHz and plot the results in Fig. 7. Kraus' empirical formula [2], which was derived based on the dominant T_1^+ mode, is added in the plot for comparison. The empirical curve implies the gain of the helix should increase as the frequency increases. However, the actual helix gain at 550 MHz is higher than

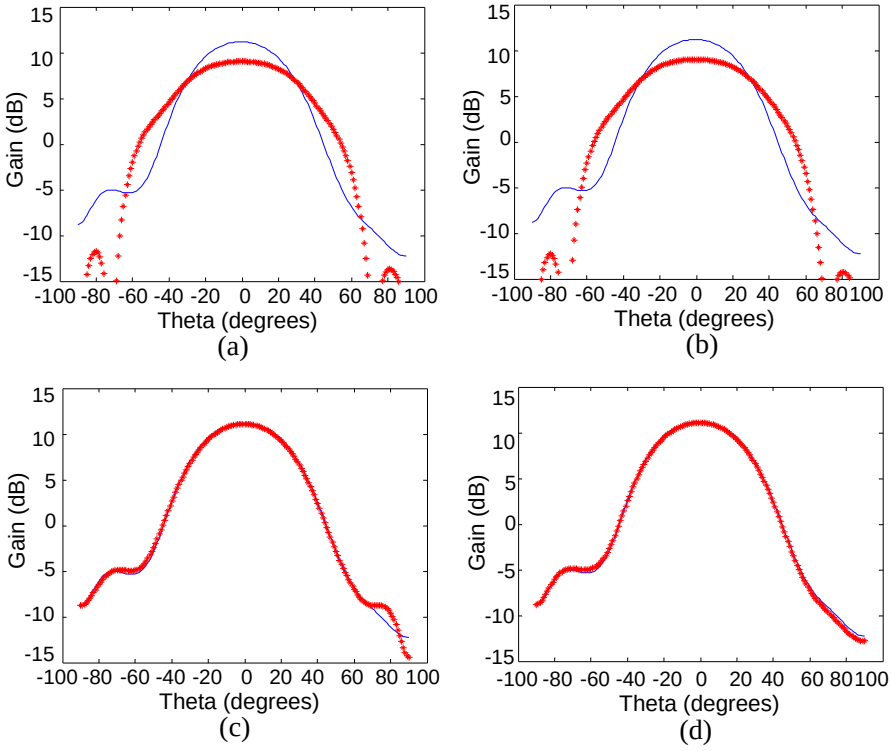

Figure 8. Gain contribution at 550 MHz. (a) T_1^+ only. (b) T_1^+ and T_1^-. (c) T_1^+, T_1^- and T_0^+. (d) T_1^+, T_1^-, T_0^+ and T_0^-.

that at 750 MHz. To better explain this result, we study the gain contribution from each current mode after the current decomposition (as illustrated earlier in Figs. 3(a)–5(a)).

Figure 8(a) plots the gain contribution of the T_1^+ mode alone at 550 MHz. It is shown as the red '+' curve and is calculated based on the T_1^+ mode extracted in Fig. 4(a). The reference curve shown in the solid blue line is the gain due to the total current simulated using NEC. It is observed that the total gain is higher than that of the T_1^+ mode alone. In Fig. 8(b), we calculate the gain contribution from both T_1^+ and T_1^-. As expected, the resulting curve does not change much from the T_1^+ mode case since the strength of T_1^- is much weaker. However, as shown in Fig. 8(c), the gain increases to the same level as the total gain when the T_0^+ mode is added in. This implies that T_0^+ contributes significantly to the gain at 550 MHz. Lastly, the T_0^- mode is added in and the resulting gain curve agrees well with the total gain, reaffirming

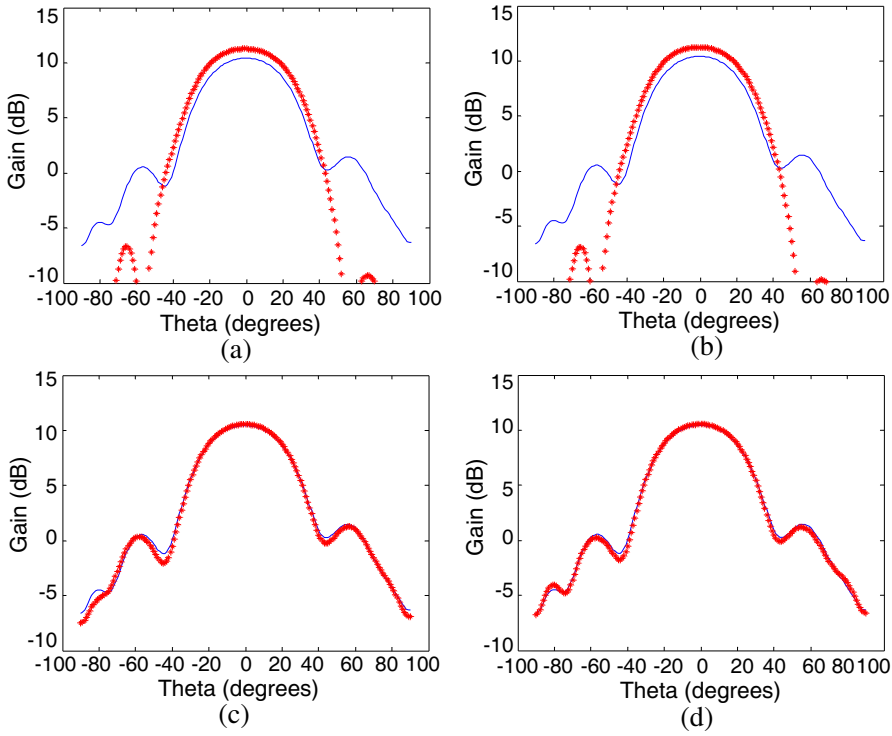

Figure 9. Gain contribution at 750 MHz. (a) T_1^+ only. (b) T_1^+ and T_1^-. (c) T_1^+, T_1^- and T_0^+. (d) T_1^+, T_1^-, T_0^+ and T_0^-.

the validity of the decomposition. Therefore, the mode by mode gain contribution study at 550 MHz clearly shows that the NEC simulated gain is higher than that of the Kraus empirical formula because T_0^+ helps the gain at low frequency. At 750 MHz, a similar procedure is carried out and Figs. 9(a)–(d) show the gain contribution from each current mode.

It is seen in Fig. 9(a) that, the gain of T_1^+ is actually higher than the total gain. But T_0^+ brings the gain curve down at this frequency, as shown in Fig. 9(c). Thus, T_0^+ hurts the gain at the center frequency. This also explains why the NEC simulated gain is lower than the Kraus's empirical formula prediction at the center frequency. The current decomposition allows us to clearly pinpoint the contribution of each mode to the gain. Consequently, we can explain why the gain at 550 MHz is higher than that at 750 MHz for a helix on an infinite ground.

3.2. Polarization

We next investigate the polarization properties of each current mode. There are eight significant current components on the helical structures, namely, T_0^+, T_1^+, T_0^-, T_1^- and their image currents $T_0^{+'}$, $T_1^{+'}$, $T_0^{-'}$ and $T_1^{-'}$. To evaluate each current mode's polarization purity, we define a polarization loss factor for the far field radiated in the endfire direction by each current component as:

$$P.L. = \frac{\vec{E} \cdot \hat{R}^*}{\left|\vec{E}\right|} \tag{3}$$

where $\hat{R}$ is a unit vector denoting the intended right-handed circular polarization (RHCP) and the * denotes complex conjugate. If the far field radiation is perfectly RHCP, *P.L.* is equal to one while if it is perfectly LHCP, *P.L.* is equal to zero. At 750 MHz, the polarization loss of all eight current components are calculated and listed in Table 1.

It is shown that, the boresight radiation of the positive traveling currents T_0^+, T_1^+ and their image currents are mostly RHCP as their *P.L.* factors are very close to one. On the other hand, the reflected currents T_0^-, T_1^- and their image currents are mostly LHCP since their

Table 1. Polarization loss of the current modes.

	T_0^+	T_1^+	T_0^-	T_1^-	$T_0^{+'}$	$T_1^{+'}$	$T_0^{-'}$	$T_1^{-'}$
P.L.	0.980	0.999	0.100	0.189	0.995	0.981	0.232	0.011

P.L. factors are closer to zero. It is very clear that both the reflected currents and their image currents are detrimental to the polarization purity of the helix. Indeed, it has been found previously that tapering the open end of the helix resulted in improved polarization purity of the helix [3]. This is because the reflected current can be reduced in the process.

4. EFFECTS OF CURRENT MODES ON TIME-DOMAIN RADIATION

Since the impedance bandwidth of the conventional helical antenna is about 2 : 1, it is a potential candidate for wideband pulse radiation [4, 5, 16]. In this section, we investigate the time-domain radiation characteristics of a helical antenna. We utilize the frequency domain results simulated via NEC over a band of frequencies as the transfer function. By multiplying the transfer function by the spectrum of the input waveform exciting the antenna, the time-domain radiation in the far field can be synthesized by the inverse fast Fourier transform (IFFT). To analyze the output time-domain waveform and gain more physical insights, we again implement a "mode by mode" decomposition described in Section 2.

A new seven-turn helical antenna with a center frequency of 750 MHz is simulated here. Again, an infinite ground plane is assumed. The circumference is one wavelength and the wire radius is 0.001 wavelength at the center frequency. The operating band of the helical antenna is from 550 MHz to 950 MHz. To find the time-domain radiation from this helical antenna, an input time pulse with uniform frequency components from 550 MHz to 950 MHz is used as

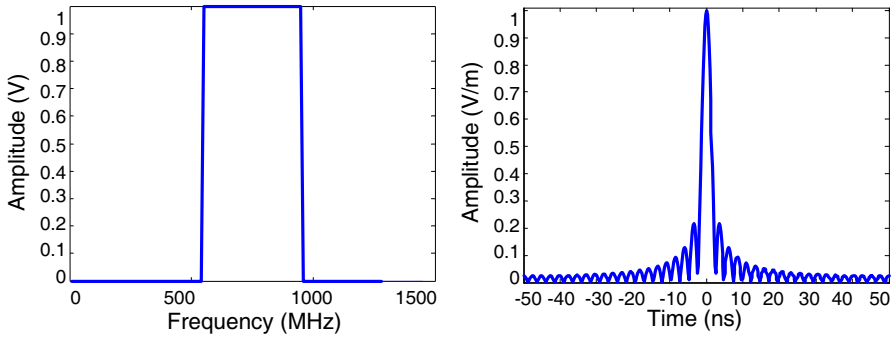

Figure 10. Input voltage wave form. (a) Frequency domain. (b) Time domain.

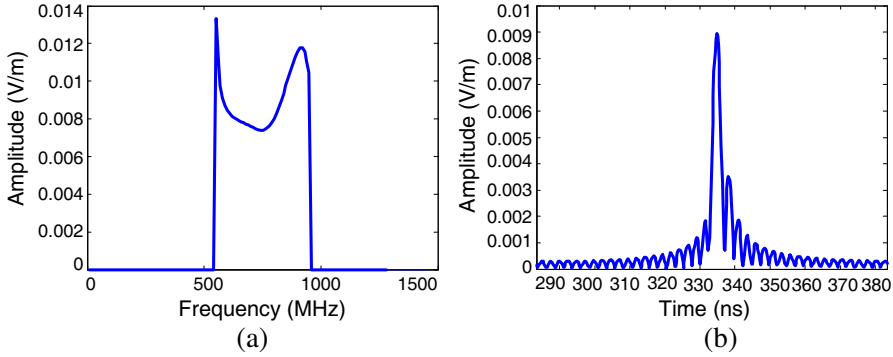

Figure 11. Output wave form at 100 m. (a) Frequency domain. (b) Time domain.

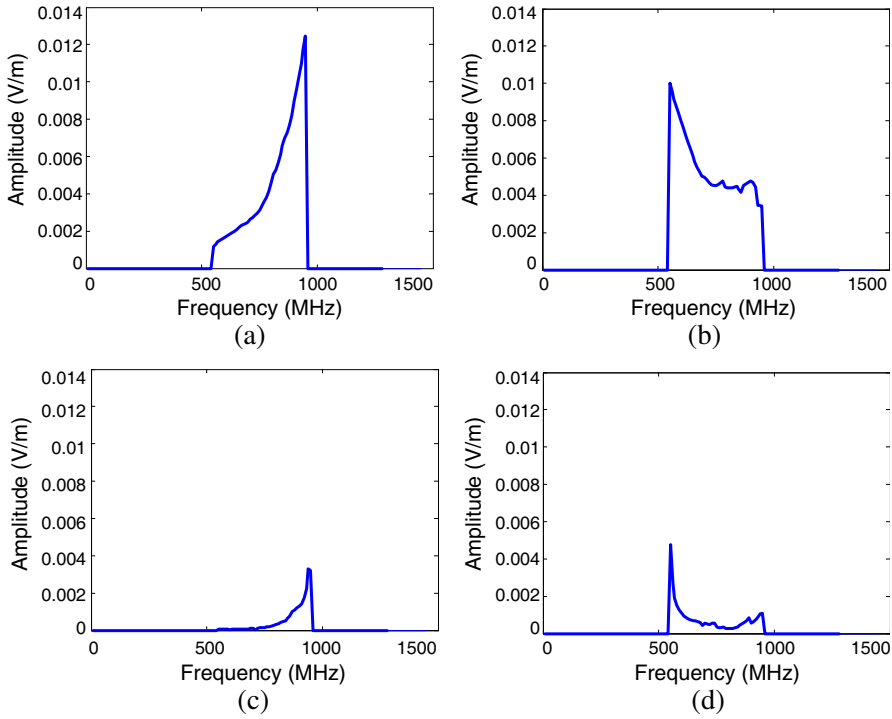

Figure 12. Mode by mode frequency domain response. (a) T_1^+. (b) T_0^+. (c) T_1^-. (d) T_0^-.

the excitation voltage on the antenna. The input waveform in the frequency domain is shown in Fig. 10(a). By applying the IFFT, the time-domain input waveform is the familiar sinc shape plotted in Fig. 10(b), with a pulse width of 2.5 ns (1/400 MHz). The radiated field from the helical antenna is recorded at 100 m away from the antenna in the axial direction. Both the frequency domain and time domain output waveforms are plotted in Figs. 11(a) and 11(b), respectively.

Compared with the input pulse in the time domain (Fig. 10(b)), the output pulse (Fig. 11(b)) appears to preserve most of the pulse shape. The time delay between the peak of the input pulse and the peak of the output pulse is 335 ns, which is approximately equal to the theoretical propagation time delay (100 m/3e8 = 333.3 ns). To estimate the strength of the radiated field, the following approximate formula can be used if we assume all quantities are fairly constant with

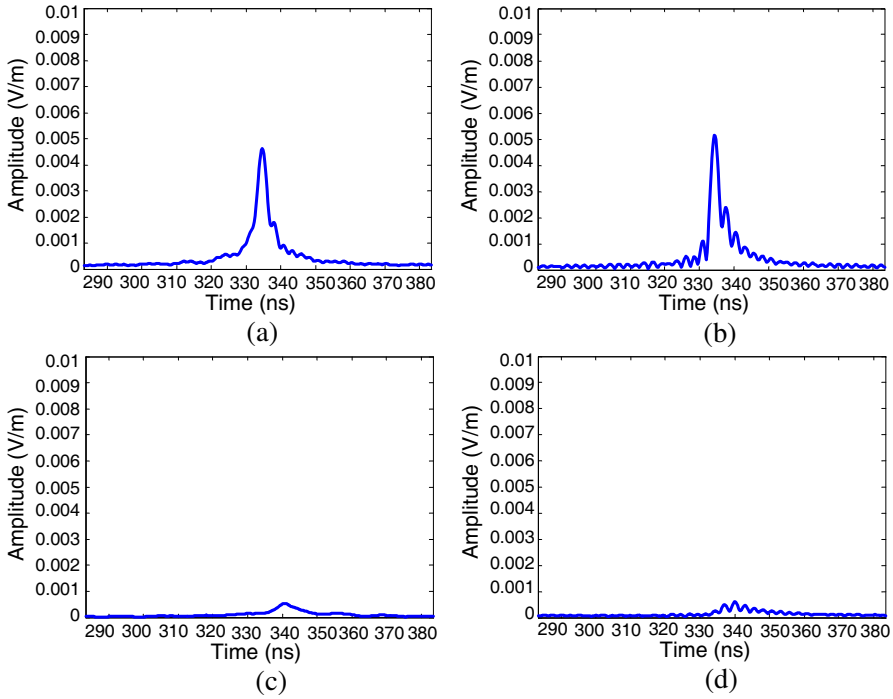

Figure 13. Mode by mode time domain response. (a) T_1^+. (b) T_0^+. (c) T_1^-. (d) T_0^-.

respect to frequency:

$$E = \sqrt{2\eta_0 \frac{V_{inc}^2}{2Z_0} \cdot \frac{(Gain)}{4\pi r^2}} \tag{4}$$

where $\eta_0 = 377\,\Omega$ is the free space wave impedance, $V_{inc} = 1\,\mathrm{V}$ is the input voltage of the helix, $Z_0 = 200\mathrm{g}\,\Omega$ is the input impedance of the helix at 750 MHz, $Gain = 8\,\mathrm{dBi}$ and $r = 100\,\mathrm{m}$. By using Eq. (3), the strength of E is predicted to be 0.0097 V/m, which is close to the peak strength of the output waveform in Fig. 11(b).

To gain more insights into the time domain response of the helix, we examine the contribution of each current mode in time. Figs. 12(a)–(d) show the individual frequency domain responses of the current modes. It is seen that the radiations of T_1^+ and T_0^+ are much stronger than the reflected components T_1^- and T_0^-. More interestingly, the T_1^+ mode radiates more at higher frequencies while T_0^+ radiates more at lower frequencies. This is consistent with the conclusion drawn from the gain study in Section 3. After the IFFT, the time domain response of each mode is generated and plotted in Figs. 13(a)–(d). It is seen that the time domain waveforms of the T_1^+ and T_0^+ have approximately the same magnitude. They add constructively in time, resulting in a well-focused time-domain radiated pulse from the helix.

5. CONCLUSION

In this paper, the ESPRIT algorithm has been applied to decompose the currents on a helical antenna. By applying ESPRIT, the strengths and phase velocities of different traveling current modes were extracted. By mapping the behaviors of these current modes across frequency, their contributions to the antenna performance including gain, polarization and time-domain pulse shape radiated from the antenna can be investigated. In terms of gain, it was found that the T_0^+ mode dominates at low frequency while the T_1^+ mode dominates at high frequency. For polarization, it was found that both the reflected components T_0^- and T_1^- and their image currents hurt the CP purity of the helical antenna. Lastly, it was found that the radiated pulse shape from a helical antenna shows only a slight dispersion. Interestingly, this is due a combination of both the T_1^+ and T_0^+ modes contributing almost equally to the wideband radiation. Therefore, it can be said that the helix is suitable for wideband (up to a 2 : 1 bandwidth) pulse applications. Although NEC was used in our study, it should be noted that currents simulated from other computer codes can be used as inputs to the decomposition. The same current

decomposition methodology can also be applied to study more complex helix structures to gain better physical insights. But it should be realized that only helical antennas with infinite ground plane can be considered. For a finite-size ground plane, the current induced on the ground cannot be easily modeled as the sum of traveling waves.

ACKNOWLEDGMENT

This work is supported in part by the National Science Foundation under grant ECCS-0725729 and the Texas Norman Hackerman Advanced Research Program under Grant No. 003658-0280-2007.

REFERENCES

1. Kraus, J. D., "Helical beam antennas for wide-band applications," *Proc. IRE*, Vol. 36, 1236–1242, Oct. 1948.
2. Kraus, J. D. and R. J. Marhefka, *Antennas for All Applications*, 3rd Edition, McGraw Hill, New York, 2002.
3. Nakano, H., *Helical and Spiral Antennas — A Numerical Approach*, Wiley and Sons, New York, 1987.
4. Mayes, J. R., W. J. Carey, W. C. Nunnally, and L. Altgilbers, "The Marx generator as an ultra wideband source," *Pulsed Power Plasma Science*, 510, 2001.
5. Giri, D. V., J. S. Levine, F. M. Tesche, and Y. Rahmat-Samii, "Numerical modeling of helical antenna excited by transient waveforms," *Directed Energy Test and Evaluation Conference*, Albuquerque, NM, 2007.
6. Maclean, T. S. M. and R. G. Kouyoumjian, "The bandwidth of helical antennas," *IRE Trans. Antennas Propagat.*, Vol. 7, 379–386, Dec. 1959.
7. Ghosh, S., A. K. Sinha, R. K. Gupta, S. N. Joshi, P. K. Jain, and B. N. Basu, "Space-harmonic effects in helical slow-wave structure — An equivalent circuit analysis," *Progress In Electromagnetics Research*, Vol. 30, 85–104, 2001.
8. Marsh, J. A., "Current distributions on helical antennas," *Proc. IRE*, Vol. 39, 668–675, Jun. 1951.
9. Roy, R., A. Paulraj, and T. Kailath, "ESPRIT — A subspace rotation approach to estimation of parameters of cisoids in noise," *IEEE Trans. Acoust., Speech, Signal Processing*, Vol. 34, 1340–1342, Oct. 1986.
10. Li, Y., H. Ling, M. Mayes, and J. Mayes, "Current decomposition

in helical antennas using ESPRIT," *IEEE Antennas Propagation Society International Symposium*, 1237–1240, San Diego, CA, Jul. 2008.

11. Wang, Y. and H. Ling, "Multimode parameter extraction for multiconductor transmission lines via single-pass FDTD and signal-processing techniques," *IEEE Trans. Microwave Theory Tech.*, Vol. 46, 89–96, Jan. 1998.
12. Li, Y. and H. Ling, "Extraction of wave propagation mechanisms in a cut-wire array using the ESPRIT algorithm," *IEEE Antennas Wireless Propagat. Lett.*, Vol. 8, 744–747, May 2009.
13. Hurst, M. P. and R. Mittra, "Scattering center analysis via Prony's method," *IEEE Trans. Antennas Propagat.*, Vol. 35, 986–988, Aug. 1987.
14. Schmidt, R. O., "Multiple emitter location and signal parameter estimation," *IEEE Trans. Antennas Propagat.*, Vol. 34, 276–280, Mar. 1986.
15. Nakano, H., Y. Samada, and J. Yamauchi, "Axial mode helical antennas," *IEEE Trans. Antennas Propagat.*, Vol. 34, 1143–1148, Sep. 1986.
16. Ghosh, D., A. De, M. C. Taylor, T. K. Sarkar, M. C. Wicks, and E. L. Mokole, "Transmission and reception by ultra-wideband (UWB) antennas," *IEEE Antennas Propagation Magazine*, Vol. 48, 67–99, Oct. 2006.